NEOPLASIA
www.neoplasia.com

Volume 18 Number 9 September 2016 pp. 541–552 541

Stromal ETS2 Regulates Chemokine Production and Immune Cell Recruitment during Acinar-to-Ductal Metaplasia[1]

Jason R. Pitarresi*,†, Xin Liu*,†, Sudarshana M. Sharma*,†, Maria C. Cuitiño*,†, Raleigh D. Kladney*,†, Thomas A. Mace*,‡, Sydney Donohue*,†, Sunayana G. Nayak*,†, Chunjing Qu#, James Lee*,†, Sarah A. Woelke*,†, Stefan Trela*,†, Kyle LaPak*,†, Lianbo Yu§, Joseph McElroy§, Thomas J. Rosol*,¶, Reena Shakya*,†, Thomas Ludwig*,†, Gregory B. Lesinski*,‡, Soledad A. Fernandez§, Stephen F. Konieczny#, Gustavo Leone*,†, Jinghai Wu*,† and Michael C. Ostrowski*,†

*Comprehensive Cancer Center, The Ohio State University, Columbus, OH 43210, USA; †Department of Cancer Biology & Genetics, The Ohio State University, Columbus, OH 43210, USA; ‡Department of Internal Medicine, The Ohio State University, Columbus, OH 43210, USA; §Department of Biomedical Informatics' Center for Biostatistics, The Ohio State University, Columbus, OH 43210, USA; ¶Department of Veterinary Biosciences, The Ohio State University, Columbus, OH 43210, USA; #Department of Biological Sciences and the Purdue Center for Cancer Research and the Bindley Bioscience Center, Purdue University, West Lafayette, IN 47907-2057, USA

Abstract

Preclinical studies have suggested that the pancreatic tumor microenvironment both inhibits and promotes tumor development and growth. Here we establish the role of stromal fibroblasts during acinar-to-ductal metaplasia (ADM), an initiating event in pancreatic cancer formation. The transcription factor V-Ets avian erythroblastosis virus E26 oncogene homolog 2 (ETS2) was elevated in smooth muscle actin–positive fibroblasts in the stroma of pancreatic ductal adenocarcinoma (PDAC) patient tissue samples relative to normal pancreatic controls. *LSL-Kras*$^{G12D/+}$; *LSL-Trp53*$^{R172H/+}$; *Pdx-1-Cre* (KPC) mice showed that ETS2 expression initially increased in fibroblasts during ADM and remained elevated through progression to PDAC. Conditional ablation of *Ets*-2 in pancreatic fibroblasts in a *Kras*^{G12D}-driven mouse ADM model decreased the amount of ADM events. ADMs from fibroblast *Ets*-2–deleted animals had reduced epithelial cell proliferation and increased apoptosis. Surprisingly, fibroblast *Ets-2* deletion significantly altered immune cell infiltration into the stroma, with an increased CD8+ T-cell population, and decreased presence of regulatory T cells (Tregs), myeloid-derived suppressor cells, and mature macrophages. The mechanism involved ETS2-dependent chemokine ligand production in fibroblasts. ETS2 directly bound to regulatory sequences for *Ccl3*, *Ccl4*, *Cxcl4*, *Cxcl5*,

Address all correspondence to: Michael Ostrowski and Jinghai Wu, Department of Cancer Biology & Genetics, The Ohio State University, 598 Biomedical Research Tower, 460 West 12th Avenue, Columbus, OH 43210.
E-mail: michael.ostrowski@osumc.edu

[1] This study was supported by National Institutes of Health grants PO1 CA097189 (M. C. O. and G. L.), NRSA F31 CA189757 (J. R. P.), and R01 CA124586 (S. F. K.). This work was also supported by the Pelotonia Fellowship Program (J. R. P.). Any opinions, findings, and conclusions expressed in this material are those of the authors and do not necessarily reflect those of the Pelotonia Fellowship Program.
Received 2 May 2016; Revised 22 July 2016; Accepted 25 July 2016

1476-5586
http://dx.doi.org/10.1016/j.neo.2016.07.006

and *Cxcl10*, a group of chemokines that act as potent mediators of immune cell recruitment. These results suggest an unappreciated role for ETS2 in fibroblasts in establishing an immune-suppressive microenvironment in response to oncogenic $Kras^{G12D}$ signaling during the initial stages of tumor development.

Neoplasia (2016) 18, 541–552

Introduction

Pancreatic cancer 5-year survival rates have remained around 5% for the last 40 years despite efforts to better understand the underpinnings of this disease [1,2]. Research for the last 2 decades has concentrated on determining the major oncogenic signaling pathways within the evolving tumor cell [3–5]. These efforts have revealed that activating mutations in *Kras* are early events during malignant transformation and have suggested that acinar cells are a potential pancreatic ductal adenocarcinoma (PDAC) cell-of-origin [6,7]. For example, genetically engineered mouse models demonstrated that mutant *Kras* targeted to the acinar lineage is sufficient to induce pancreatic intraepithelial neoplasia (PanIN) lesions with ductal morphology [8–10]. Additionally, second-hit mutations, such as activating Notch mutations, synergize with Kras in acinar cells to drive ductal reprogramming and PanIN lesion formation [11]. Lineage tracing experiments have shown that acinar cells readily transdifferentiate into ductal cells (commonly referred to as acinar-to-ductal metaplasia or ADM) and also demonstrated that oncogenic *Kras* mutations in mature acinar cells formed PanINs at a significantly higher frequency relative to the ductal or centroacinar cell lineages [12]. This paradigm-shifting study has sparked newfound interest into the signaling networks that collaborate with *Kras* to drive ADM in acini [13–17]. Other reports have solidified the notion that ADM progresses to PanIN and PDAC and show that ADM occurs in human PDAC patients [18–21]. During the transformation from ADM to PanIN to PDAC, there is a concurrent increase in the desmoplastic reaction that is a cardinal feature of this disease [22–24].

The pancreatic stroma has been scrutinized as a "partner in crime" for PDAC development, but efforts to elucidate the role of the stroma in pancreatic cancer to date have relied primarily on *in vitro* or transplanted immunodeficient *in vivo* models of pancreatic cancer [25–28]. More recent reports have revealed that stromal fibroblasts are comprised of a heterogeneous population that possesses both pro- and antitumor characteristics [29–31]. For example, the presence of smooth muscle actin (SMA)–positive fibroblasts in human PDAC samples has been correlated with reduced overall survival in one patient cohort and with increased patient survival in an independent patient cohort [31,32]. Furthermore, stromal gene expression in 145 human PDAC patient samples revealed two distinct stroma-specific subtypes (termed *normal* and *activated*) with median survivals of 24 or 15 months, respectively [33]. Collectively, these observations have fueled interest in studying the molecular interactions between the epithelium and recruited stromal fibroblasts. Surprisingly, the contribution of fibroblasts to ADM has not garnered the same attention, and noncell autonomous signaling that drives ADM is not well described.

ETS2 is a member of the ETS transcription factor family that has been studied as a downstream regulator of RAS-mediated transformation [34–37]. ETS2 also interacts specifically with mutant p53 to redirect promoter recruitment of p53, and further studies have shown that ETS2 is crucial for mutant tp53 oncogenic functions [38–40]. The ability of ETS2 to regulate both RAS- and p53-mediated signaling places it at a crossroads between these two powerful oncogenic signaling pathways that are misregulated in pancreatic cancer. Previous studies have revealed that ETS2 also regulates epithelial cell fate from the stromal compartment [41,42]. Specifically, deletion of *Ets2* in the epithelium of mouse mammary tumor models had no significant effect, whereas fibroblast-specific *Ets2* deletion led to markedly decreased tumor growth [42]. These studies have established that fibroblast ETS2-mediated signaling is an important regulator of the complex cross talk between stromal cells and epithelial cells. ETS factors in general (especially ETS1 and ETS2) are enriched in stromal cell populations in many cancers through a variety of mechanisms [41,43–46].

In this report, we show that ETS2 signaling is activated in human and mouse pancreatic fibroblasts during ADM. We further use genetically engineered mouse models of ADM to demonstrate that deletion of *Ets-2* in fibroblasts leads to decreased acinar cell transformation, decreased immune cell infiltration, and decreased cytokine and chemokine production by fibroblasts. These results define a fibroblast-specific ETS2-choreographed immune response that leads to an immune-suppressive microenvironment during the earliest stages of preneoplastic transformation of the pancreas.

Materials and Methods

Animal Strains, Husbandry, and Maintenance

The use of animals was in compliance with federal and Ohio State University Laboratory Animal Resources regulations. $Mist1^{KrasG12D}$; *Fsp-Cre;* $Ets2^{db/loxP}$ *and* $Mist1^{KrasG12D}$; $Ets2^{db/loxP}$ animals were generated by crossing the previously described $Mist1^{KrasG12D}$, *FspCre,* $Ets\text{-}2^{loxP}$, and $Ets\text{-}2^{db}$ strains [10,47–49]. The experiments were performed using littermate mice from a mixed C57BL/6; 129/Sv and FVBN genetic background.

Multispectral Analysis of Dual-Color Immnohistrochemistry (IHC)

Dual-stained samples were imaged using the PerkinElmer's Vectra multispectral slide analysis system. For the mouse samples, at least three multispectral images per animal for at least three mice per genotype (unless otherwise noted) were manually taken. For the human PDAC Tissue Microarray, one field of interest per core was automatically acquired. The image acquisition workflow consisted of the following: 1) monochrome imaging of the entire slide, 2) RGB low-power imaging of the tumor tissue using an inForm tissue finding algorithm, and 3) multispectral high-power imaging of one field containing tumor epithelium and stroma by means of an inForm HPF finding algorithm.

For quantification of the DAB staining, the multispectral images were reviewed and analyzed using inForm Tissue Finder software. A pattern recognition algorithm was used for processing as follows: 1) trainable tissue

segmentation to segment the SMA-positive regions from the tumor epithelium; 2) cell segmentation of the SMA-positive tissue category to locate the subcellular compartments; and 3) scoring to bin the spectrally unmixed DAB signal into four categories depending on the staining intensity (0+, 1+, 2+, and 3+), providing data in percent. The H-score, which ranges from 0 to 300, was calculated using following formula: [1 × (% cells 1+) + 2 × (% cells 2+) + 3 × (% cells 3+)]. Thus, H-score measures staining intensity as well as percentage of positive cells in a given cellular compartment.

Histology Analysis, Immunohistochemistry, and Immunofluorescent Staining

Dissected mouse pancreas tissues were fixed in 10% neutral-buffered formalin solution for 48 hours and transferred to 70% ethanol. Tissues were processed, embedded in paraffin, cut in 5 μm sections on positively charged slides, deparaffinized, rehydrated, and stained with hematoxylin and eosin (H&E).

For immunohistochemistry, all sections were stained using a Bond Rx autostainer (Leica) unless otherwise noted. Briefly, slides were baked at 65°C for 15 minutes, and automated software performed dewaxing, rehydration, antigen retrieval, blocking, primary antibody incubation, post primary antibody incubation, detection (DAB or RED), and counterstaining using Bond reagents (Leica). Samples were then removed from the machine, dehydrated through ethanols and xylenes, mounted, and coverslipped. Antibodies for the following markers were diluted in antibody diluent (Leica): rabbit anti-bodies αSMA (1:1500, Abcam), Ki67 (1:100, Abcam), and amylase (1:400, CST), ETS2 (SC-351) and rat antibodies cytokeratin 19 (TROMA-III) (1:150, DSHB, University of Iowa), and F4/80 (1:50 Invitrogen).

For fluorescent immunostaining, following deparaffinization, rehydration, and PBS washes, sections were blocked with serum-free Protein block (Dako) for 30 minutes at room temperature. Cells grown on coverslips were fixed with 4% paraformaldehyde and permeabilized with 100% ice-cold methanol prior to blocking. Tissue immunostaining required antigen retrieval, which was performed in a steamer (Black & Decker) using a 1× Target Retrieval solution (pH 6.0) (Dako). Antibodies for the following markers were diluted in antibody diluent (Dako) and applied overnight at 4°C: rabbit antibodies Ki67 (1:100, Abcam) and amylase (1:400, CST), rat antibodies cytokeratin 19 (TROMA-III) (1:150, DSHB, University of Iowa) and cytokeratin 8 (TROMA-I) (1:300, DSHB, University of Iowa), and mouse antibody α-SMA (1:400 Sigma). Secondary antibodies conjugated with Alexa Fluor 488 and Alexa Fluor 594 were placed on tissue sections for 1 hour at room temperature (1:300, Invitrogen). Nuclei were counterstained using SlowFade Gold Antifade reagent with 4′,6-diamidino-2-phenylindole (Invitrogen). Tissue sections for fluorescence microscopy images were mounted with SlowFade Gold Antifade reagent with 4′,6-diamidino-2-phenylindole (Invitrogen) and coverslipped, and images were obtained using an Eclipse E800 microscope (Nikon) equipped with a CoolSNAP cf. monochrome digital camera Peltier cooled to 20°C (Photometrics). All images were captured with MetaVue version 6.2r6 software (Universal Imaging Corp.) and resized and formatted with Adobe Photoshop CS5 software (Adobe Systems Incorporated).

Chromatin Immunoprecipitation (ChIP) Assays

ChIP assays were performed as previously described [43]. Briefly, cells were cross-linked for 10 minutes with 1% formaldehyde and lysed. Chromatin was collected and sonicated. Anti-Ets2 ChIP grade antibody (sc-351X) and protein G agarose slurry (Millipore 16-266) were used to pull down chromatin. After reverse cross-linking, DNA was recovered, purified, and analyzed by reverse transcriptase polymerase chain reaction (RT-PCR).

Pancreatic Fibroblast Isolation and Culture

Primary pancreatic fibroblasts were purified based on the following protocol. Briefly, pancreata were dissected from 6-month-old mice, minced, and digested with collagenase (0.5% Collagenase II, 120 U ml^{-1} DNase I in 1× PBS) shaking at 225 rpm for an hour at 37°C. Collagenase was neutralized with 10% FBS-Dulbecco's modified Eagle's medium. Digested tissue was resuspended in medium and gravity purified for 10 minutes. Supernatants were aspirated, and pellets were washed three times and subjected to two additional gravity sedimentations and then seeded on tissue-culture dishes.

RNA, Microarray, and Real-Time PCR

RNA was harvested with Trizol according to the manufacturer's instructions (Invitrogen). RNA quality and concentration were assessed with Bioanalyser and Nanodrop RNA 6000 nanoassays. RNA samples were hybridized to Affymetrix GeneChip Mouse genome 430 2.0 platform at the Microarray Shared Resource Facility, Ohio State University Comprehensive Cancer Center. The microarray data were deposited with Gene Expression Omnibus (GEO) and can be viewed at http://www.ncbi.nlm.nih.gov/geo/query/acc.cgi?token=afqbqaeoxbgltor&acc=GSE61707.

The RNA-sequencing data were deposited with GEO under Series GSE76498 and can be viewed at http://www.ncbi.nlm.nih.gov/geo/query/acc.cgi?token=mlwjyqiqplmfbyd&acc=GSE76498. Real-time quantification of mRNA was performed using Roche Universal Primer Library probes and probe-specific primers. Applied Biosystems StepOnePlus real time PCR machines were used. Normalization and target to reference ratios were calculated according to the manufacturer's instructions (Roche). Total RNA (1 μg) was converted to cDNA using the Super-script Reverse Transcriptase kit (Invitrogen). List of quantitative (q)RT-PCR and Roche Universal Probe library number is indicated in the table below:

Gene Name	Forward Primer	Reverse Primer	Probe #
hRpl4	AGCGTGGCT GTCTCCTCTC	GGACCCATCAAA GGTGTCAA	40
hEts2	CCCCTGTGGCT AACAGTTACA	AAGGGAGCACA GCAAACAGA	20
hGli1	CAGGGAGGAAA GCAGACTGA	ACTGCTGCAGG ATGACTGG	76
hGli2	ACTCCACACAC GCGGAAC	CCACTGAAG TTTTCCAGGATG	16
hGli3	TCAAACCCGAT GAAGACCTC	TTGTTCCTT CGGGCTGTT	26
hStat3	CCTCTGCCGG AGAAACAG	CTGTCACTGTA GAGCTGATGGAG	1
hJun	CCAAAGGATAGT GCGATGTTT	CTGTCCCTCTCC ACTGCAAC	19
hMyc	CGGTTTTC GGGGCTTTAT	GGCTCTTCCA CCCTAGCC	13
hSox11	GAGCTGAGC GAGATGATCG	GAACACCAGGT CGGAGAAGT	19
hMed1	AACACCCTCA TTGGAAGCTG	GGACACACTTC AAATTGGAGAA	2
hp65	CGGGATGGC TTCTATGAGG	GGATGCGCT GACTGATAGC	1
mRpl4	GATGAGCTGTAT GGCACTTGG	CTTGTGCAT GGGCAGGTTA	38
mCcl3	TGCCCTTG CTGTTCTTCTCT	GTGGAATCTT CCGGCTGTAG	40
mCcl4	AGGAGGAGCC ACTTCAGGA	GAGCAAGGACG CTTCTCAGT	73
mCxcl4	AGCGGTGGTT GCTGTCAC	TGGTGATGTG CTTAAGATGGA	82
mCxcl5	TAGAGCCCC AATCTCCACAC	GAGCTGGAGG CTCATTGTG	67
mCxcl10	GCTGCCGTC	TCTCACTGG	3

(continued on next page)

(*continued*)

Gene Name	Forward Primer	Reverse Primer	Probe #
chipCcl3	ATTTTCTGC GTCCTACCTCCT CCTGCTCA	CCCGTCATC TCAGCTCTCAA CTCGTGACC	60
chipCcl4	CCACTCCATCT CCCTCCTTT	GAAAGTGAGGA GTTCCTGACAGA	3
chipCxcl4	CACATCTCCAA CCCCACAG	CACGTAACTCC AAAGCCACTG	4
chipCxcl5	GGCAAAGGG TGCAAAGATT	CAACTTCACAG ATGACTCAGCA	69
chipCxcl10	CTCAGCGGT GGATGAAGC	GGACTCAGGG AGGGAAACTC	73
hCcl3	TCTTCCTAACC AAGCGAAGC	GAAGCTTCT GGACCCCTCA	1
hCcl4	CTCTCCAGCG CTCTCAGC	ACCACAAAGTT GCGAGGAAG	40
hCxcl4	ACTGAGATCCT GCTGGAAGC	AAGTGGCAGG AGCAGCAA	66
hCxcl5	TGACACTTGT GAAAAGGCTTGTA	AGCAAAAATAG AAATTCACAACCA	52
hCxcl10	GATGCAGTG CTTCCAAGGAT	TGACATATACTCC ATGTAGGGAAGTG	34

Statistics

Wilcoxon rank sum test and Student's *t* test were calculated using R 3.0.1. The *P* values from Student's *t* tests are listed unless otherwise specified. In all graphs, median, means (bar), and standard deviations (lines) are denoted. Microarray data were processed by Robust Multiarray Average method and analyzed using the moderated *t* test approach [50]. *P* value of .05 was considered significant.

Results

Ets-2 Signaling Is Activated in Pancreatic Fibroblasts

Previous studies have shown that ETS2 levels increase in ductal tumor cells with PDAC staging, but fibroblast ETS2 levels have yet to be explored [51]. Dual-color IHC staining of normal pancreatic tissue, pancreatitis tissue, and PDAC patient tissue for alpha-SMA and ETS2 was analyzed using the Vectra multispectral imaging system (Figure 1*A*, see Materials And Methods). The analysis demonstrated that nuclear ETS2 staining was significantly enriched in fibroblasts from both pancreatitis and PDAC patient samples relative to normal pancreatic controls (Figure 1*B*). Robust staining within acinar and ductal epithelial cells in both normal and PDAC patient samples was also observed, consistent with previous reports [51]. To further test the hypothesis that ETS2 is activated in pancreatic fibroblasts, primary fibroblasts from resected PDAC patient tumors were isolated, and mRNA expression of *Ets-2* was compared relative to other proto-oncogenic transcription factors. Among the 10 transcription factors analyzed, only *Ets-2* and *Gli1* showed significantly higher levels of mRNA in cancer-associated fibroblasts relative to control pancreatic fibroblasts (Figure 1*C*). *Gli1*, the nuclear effector of Hedgehog receptor signaling, has been previously shown to be expressed by pancreatic cancer–associated fibroblasts [52,53].

Fibroblast Ets-2 Is Upregulated Early and Late in Pancreatic Tumorigenesis

SMA-ETS2 dual IHC was repeated in a cohort of *LSL-Kras*$^{G12D/+}$*; LSL-Trp53*$^{R172H/+}$*; Pdx-1-Cre* (KPC) mice, demonstrating that ETS2 is activated in fibroblasts during early ADM and PanIN stages (2 weeks of age) as well as in PDAC (4 months of age, Figure 2, *A* and *B*). Gene set enrichment analysis (GSEA) of RNA sequencing of fibroblast mRNA isolated from WT or KPC pancreata at the ADM stage demonstrated that extracellular matrix remodeling and inflammatory response pathways were highly enriched in KPC fibroblasts relative to WT fibroblasts (Figure 2*C*). GSEA also identified ETS2-regulated genes as an altered process in fibroblasts isolated from KPC mice undergoing ADM (Figure 2*C*). This same ETS2 GSEA pathway ("RYTTCCTG_V$ETS2_B" Broad Institute MSigDB gene set) was significantly altered ($P = 1.68 \times 10^{-4}$) in the "activated stroma" signature relative to "normal stroma" in the recent analysis of stromal gene expression from 145 PDAC patients [33].

Fibroblast-Specific Deletion of Ets-2 Decreases Kras^{G12D}*-Driven ADM*

To determine the role of *Ets2* signaling in epithelial-stromal cross talk during ADM formation, we utilized the *Mist1*^{KrasG12D} knock-in allele in which oncogene expression originates in the acinar cell compartment [10]. This model was combined with fibroblast-specific *Fsp-Cre,* which was previously created and characterized extensively by our group [41,42], and *Ets2*$^{db/loxP}$ alleles to achieve efficient fibroblast-specific conditional deletion of *Ets-2*. *Mist1-Kras*^{G12D}*; Ets2*$^{db/loxP}$ (**KE**) control mice and *Mist1-Kras*^{G12D}*; Fsp-Cre; Ets2*$^{db/loxP}$ (**KCE**) experimental mice were generated (Supplemental Figure 1*A*, see Materials and Methods). Recombination of the *Ets2*^{loxP} allele was confirmed in DNA isolated from formalin-fixed, paraffin-embedded tissue sections by genotyping PCR (Supplemental Figure 1*B*). IHC staining and quantification using Vectra multispectral imaging of ETS2 in pancreatic tissue sections from KE and KCE mice confirmed *in vivo* deletion exclusively in the fibroblast compartment (Supplemental Figure 1, *C* and *D*), whereas ETS2 levels in the pancreatic epithelium remained unchanged (Supplemental Figure 1*E*). Pancreatic fibroblasts were isolated from KE and KCE mice and shown to be positive for fibroblast markers SMA and vimentin and negative for epithelial markers cytokeratin 8 (CK8) or cytokeratin 19 (CK19) by co-immunofluorescence (co-IF) (Supplemental Figure 1*H*). KCE fibroblast cultures had lower *Ets-2* mRNA relative to KE (Supplemental Figure 1*I*), and genotyping PCR was performed to show deletion of *Ets-2*^{loxP} exclusively in cultures isolated from *Fsp-Cre*–bearing mice (Supplemental Figure 1*J*).

To further confirm the fibroblast specificity of the *Fsp1-Cre* in the pancreas, as previously demonstrated in normal mammary gland and mammary tumors [41,42], we performed co-IF staining with the macrophage marker F4/80 and ETS2. Consistent with our published reports, there was no difference in ETS2 staining in F4/80 macrophages between KE and KCE mice (Supplemental Figure 1, *F* and *G*). These collective results indicate that *Ets-2* is efficiently deleted in KCE mice exclusively in the fibroblast compartment and this deletion is maintained under *in vitro* culture conditions.

Ets-2 specific deletion in stromal fibroblasts significantly decreased the amount of ADM events, identified by ducts that stain positive for ductal cell marker CK19 and acinar cell marker β-amylase (Figure 3, *A* and *B*). CK19/Ki67 co-IF staining showed that ductal cells in KCE mice had two-fold lower proliferation than KE lesions (Figure 3, *C* and *D*; matched H&E in Supplemental Figure 2*A*). Staining with apoptosis marker cleaved caspase 3 showed increased numbers of apoptotic epithelial cells in the preneoplastic ADMs in KCE mice relative to KE (Figure 3, *E* and *F*).

Ets-2 Deleted Fibroblasts Are Viable and Maintain an Activated Phenotype

Gene expression analysis of *Ets2*-intact and *Ets2*-deleted fibroblast revealed that loss of *Ets2* in pancreatic fibroblasts led to significant changes (Supplemental Figure 3*A* and Supplemental Table 1).

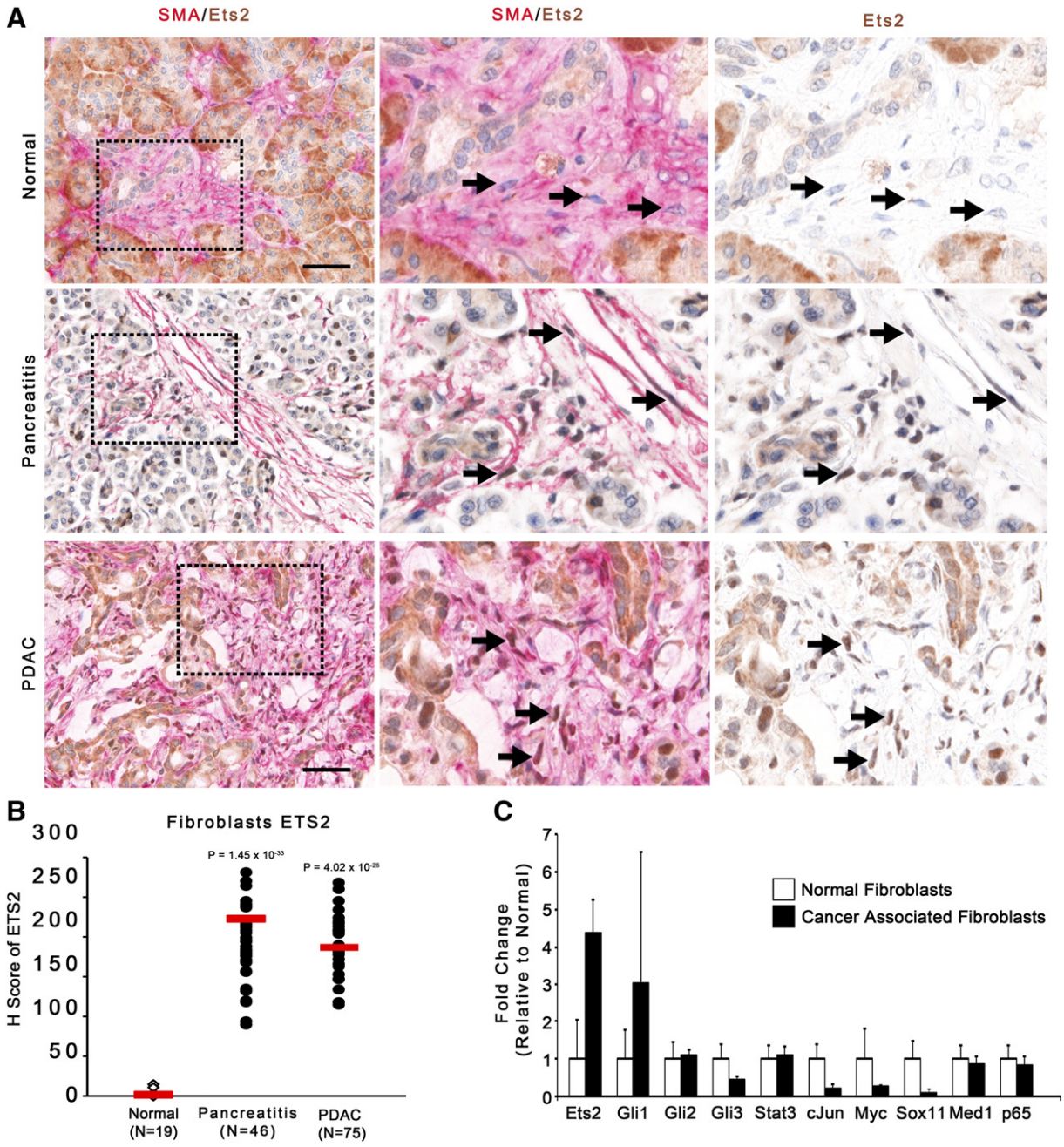

Figure 1. Human pancreatic cancer associated fibroblasts activate Ets-2 signaling.(A) Dual-color IHC (ETS2, brown; SMA, red) of human normal or PDAC Tissue Microarray. Insets show higher magnified view of representative areas. Black arrows indicate ETS2+/SMA+ fibroblasts. Scale bars 25 μm. (B) Quantification of ETS2 staining in SMA+ positive cells shown in A (red bar indicates mean). (C) qRT-PCR analysis of proto-oncogenic transcription factors in pancreatic fibroblasts isolated from normal or PDAC patients (normalized to *Rpl4,* represented as fold-change relative to normal fibroblast expression; $n = 3$; bars represent means ± Standard Deviation [SD]).

GSEA identified the ETS2 target gene signature as significantly downregulated in the KCE versus KE fibroblasts (Figure 4*A*, $P = .002$). However, in contrast to our findings in breast cancer [42], GSEA indicated that pancreatic fibroblasts lacking *Ets-2* maintained an activated extracellular matrix (ECM) remodeling state, as there was no significant difference between KCE and KE fibroblasts (Figure 4*B*; $P = .117$ and false discovery rate [FDR] > 25%). In contrast, GSEA identified that inflammatory responses were significantly affected by *Ets2* deletion in fibroblasts (Figure 4*C*, $P < .001$).

Dual-color IHC staining of SMA and Ki67 showed no difference in the proliferation or total number of SMA-positive fibroblasts in KCE mice compared to KE controls, demonstrating that differences in ADM formation between KE and KCE mice were not due to decreased viability or proliferation of *Ets2*-null fibroblasts (Figure 4*D* and Supplemental Figure 3*B*, respectively). An important physiological function for activated stromal fibroblasts is to form and remodel a collagen-rich extracellular matrix. Masson's Trichrome staining revealed no significant difference in the area of collagen-rich ECM between KCE and KE mice, consistent the

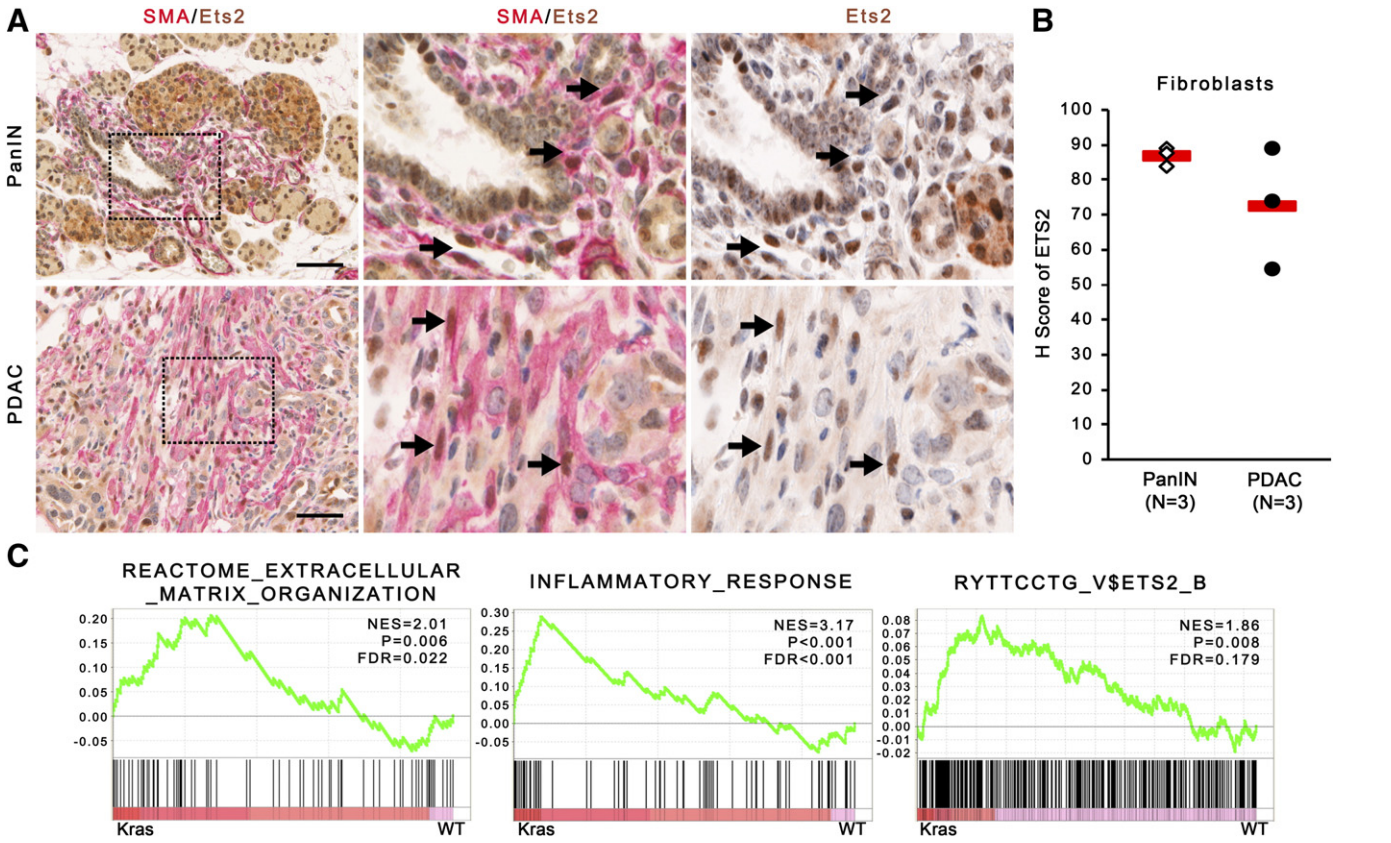

Figure 2. ETS2 is upregulated in PanIN and PDAC fibroblasts.(A) Dual-color IHC (ETS2, brown; SMA, red) of pancreata from KPC mice at PanIN or PDAC stage. Insets show higher magnified view of representative areas. Black arrows indicate ETS2+/SMA+ fibroblasts. Scale bars 25 μm. (B) Quantification of ETS2 staining in SMA+ positive cells shown in A (red bar indicates mean). (C) GSEA enrichment plots for ECM remodeling, inflammation, and ETS2-regulated gene pathways in mouse WT or KPC pancreatic fibroblast cultures ($n = 3$).

GSEA prediction (Figure 4, *F* and *G*). Similarly, GSEA showed no difference in angiogenesis pathways between KE and KCE fibroblasts (Supplemental Figure 3*C*; $P = .174$ and FDR > 25%), and Meca-32 staining of endothelial cells demonstrated no significant differences between control and ETS2-null tissue (Supplemental Figure 3*D*).

Ets-2 Deletion In Fibroblasts Alters the Immune Cell Infiltrate during ADM

To explore the predicted changes in inflammatory responses upon *Ets2* deletion in pancreatic fibroblasts, antibodies for cell-type–specific markers were used to test whether KE and KCE mice had different infiltration of GR1-positive myeloid-derived suppressor cells (MDSCs), F4/80-positive macrophages, FoxP3-positive Tregs, or CD8-positive cytotoxic T cells. The results demonstrated that MDSCs, Tregs, and macrophages were recruited to the stroma in KE mice, and all three cell populations were significantly depleted in the KCE mice with *Ets2* ablation (Figure 5, *A–D* and Supplemental Fig. 4, *A* and *B*, respectively). Of note, recruitment of MDSCs into the pancreatic stroma of KCE mice was decreased by 100-fold compared to KE mice (Figure 5*A*). In contrast, CD8+ cytotoxic T cells were increased two-fold in KCE mice compared to KE controls (Figure 5, *E* and *F*). CD8+ cells were confirmed to be dual positive for CD3 (Figure 5*G*; *white arrows*).

Ets-2 Directly Regulates Chemokine Expression in Pancreatic Fibroblasts

GSEA revealed that chemokine and cytokine pathways were significantly affected by Ets2 deletion (Figure 6*A*). Further *in silico* dissection of the chemokine and cytokine GSEA pathways showed that 15 secreted factors were present on the leading edge analysis of the pathways (Supplemental Table 2). The 15 ligands belonged to 3 subgroups: chemokine ligands, interleukins, and TNF superfamily members (Supplemental Table 3). Using publically available data on the Encyclopedia of DNA Elements consortium database, we used ChIP-Seq data available for the closely related transcription factor ETS1 (GEO accession GSM1003774 and GSM1003777) to identify predicted ETS binding sites in the promoters of the 15 ligands. The promoters of 9 of the 15 factors (60%) contained ETS1 ChIP-Seq peaks that are also predicted ETS2 binding sites (Supplemental Table 3). The ETS2 binding sites were conserved in mice and human (Supplemental Figure 5). Out of these nine, five factors (CCL3, CCL4, CXCL4, CXCL5, CXCL10) are known to function in recruiting T cells, macrophages, or MDSCs [54–58] (Supplemental Table 3).

Strikingly, real-time RT-PCR confirmed that mRNAs for all five ligands were expressed in KE fibroblasts, whereas expression was not detectable in cells with *Ets2* deletion (Figure 6*B*). Furthermore, all five ligands were expressed in human PDAC patient-derived cancer associated fibroblasts (Figure 6*C*). ETS2 ChIP on chromatin from KE and KCE pancreatic fibroblasts showed significant ETS2 enrichment in ETS2-intact versus deleted fibroblasts (Figure 6*D*).

Discussion

The results presented here identify ETS signaling in fibroblasts as a means of immune cell recruitment to ADM. ETS2 directly coordinates a chemokine signature that alters the immune contexture at the early

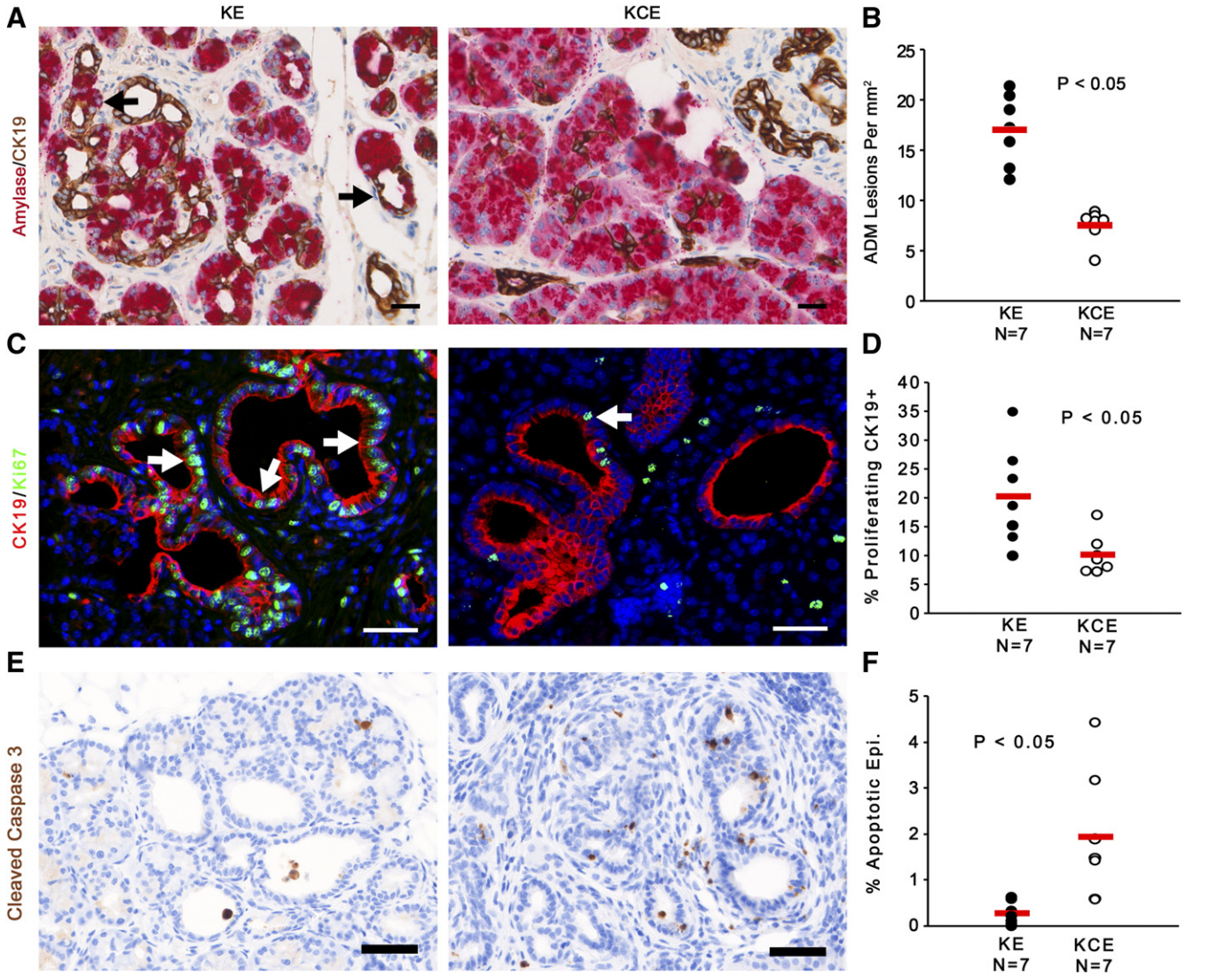

Figure 3. Stromal ETS2 ablation decreases pancreatic ADM.(A and B) Dual-color IHC and quantitation for β-amylase (red) and CK19 (brown). Black arrows indicate ADM lesions. (C and D) Co-IF for CK19 (red) and Ki67 (green) and quantification of percentage of proliferating CK19+ cells, indicated by white arrows. (E and F) IHC for cleaved caspase 3 (brown) and quantification of percentage of epithelial cells undergoing apoptosis. All scale bars 25 μm (n = 7; red bar indicates mean).

ADM stage. Loss of ETS2 signaling in the pancreatic stroma abrogates production of key chemokines in fibroblasts, resulting in decreased infiltration of macrophage, MDSC, and Treg populations while increasing CD8 T cells.

The stroma undergoes a dramatic expansion in concert with the stepwise development of pancreatic cancer, suggesting that the stroma is an active partner in disease initiation and progression. However, characterizing the complex interactions between the pancreatic epithelium and the adjacent stroma has proved difficult, as recent reports have highlighted the degree of heterogeneity that exists in the pancreatic stroma. In particular, depletion of SMA-positive cells accelerated pancreatic cancer, whereas depletion of FAP-positive cells slowed tumor growth [29,31]. Interestingly, both studies identified immune cell subpopulations that dynamically interact with stromal fibroblasts. Tumors depleted for SMA-positive cells were responsive to α-CTLA-4 therapy, which functions by altering T-cell activation [31]. Tumors depleted for FAP-positive cells were dependent on both CD4 and CD8 T-cell populations, and fibroblast depletion synergized with α-PD-1 and α-CTLA-4 immune checkpoint therapy [29]. These studies indicate that fibroblast-immune cell cross talk is complex, and our results establish that ETS2 is responsible for the production of several key immunomodulatory chemokines and cytokines. We propose that ETS2 is activated in fibroblasts early during epithelial transformation of the pancreas and helps to establish an immune microenvironment that is conducive to increased ADM formation.

The function of ETS2-mediated signaling in pancreatic fibroblasts is to modulate the presence of immune cells in the preneoplastic stroma and is a phenotype that is distinct from its role in mammary fibroblasts. Our previous studies in mammary tumor growth have shown that the primary function of ETS2 in the fibroblast compartment is to promote angiogenesis, which was not observed in the pancreas [41,42]. Furthermore, differences in chemokine and cytokine gene expression and changes in immune cell populations

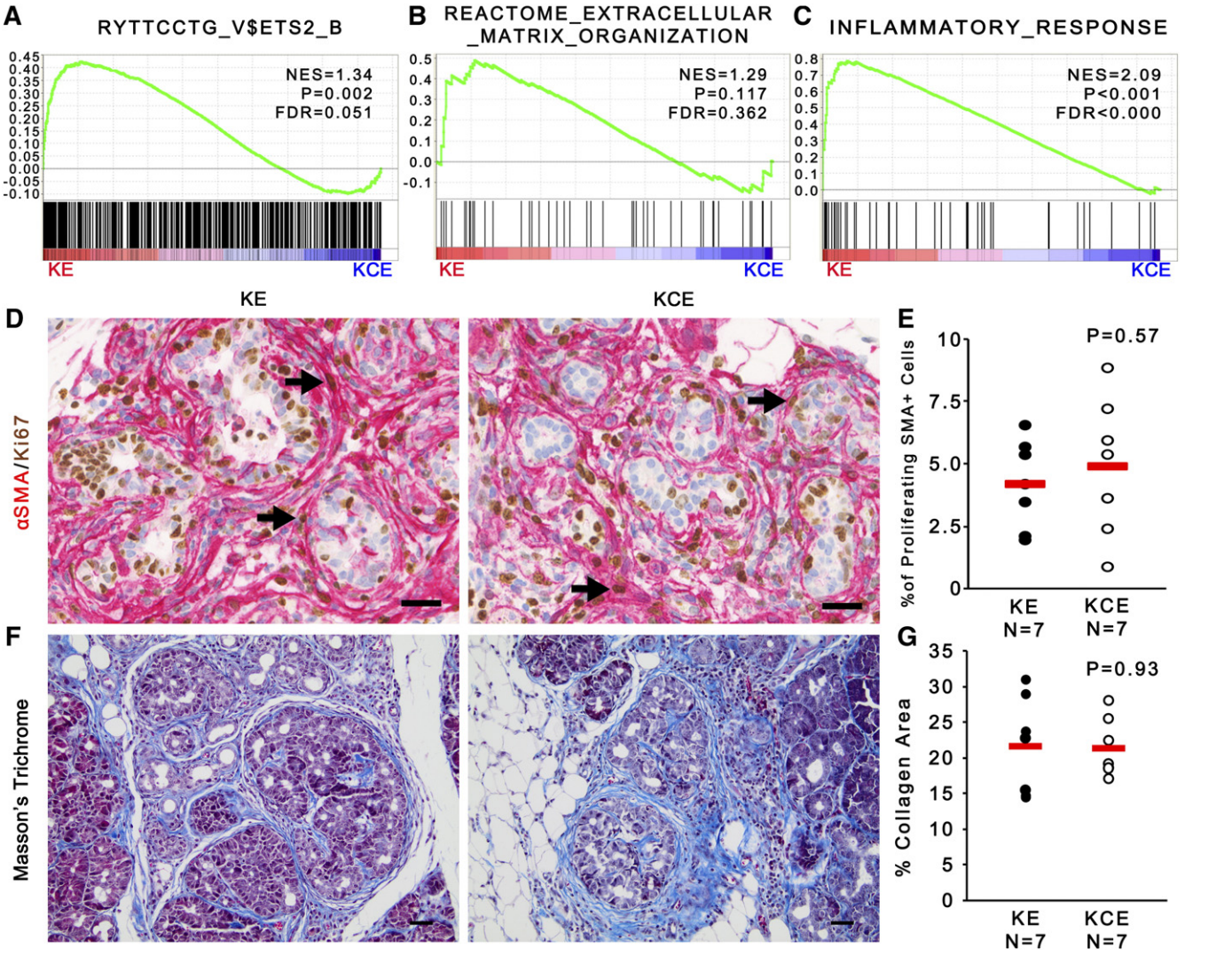

Figure 4. *Ets-2* deletion does not affect fibroblast proliferation or collagen deposition.(A–C) GSEA enrichment plots for Ets2-regulated genes, ECM remodeling, and inflammation pathways in KE and KCE fibroblasts ($n = 3$). (D and E) Dual-color IHC of SMA (red) and Ki67 (brown) and quantification showing the percentage of proliferating SMA+ cells, indicated by black arrows. (F and G) Masson's Trichrome stain and quantification of the percent area of collagen staining ($n = 7$; red bar indicates mean).

identified in this work were not observed with *Ets2* loss in the breast tumor stroma [41,42]. Thus, ETS2 alters the fibroblast transcriptome in a tissue-specific fashion and subsequently modulates the communication between the epithelial cell and its microenvironment in distinct manner. This is consistent with the observation that fibroblasts maintain a complex positional memory that drives specific gene expression patterns based on their topographical location [59]. These results also highlight the diversity of stromal fibroblasts and show that a more detailed understanding of the signaling networks within fibroblasts derived from cancers of different origins is required to more precisely understand epithelial-fibroblast cross talk.

The most striking change in immune cell recruitment upon loss of ETS2 signaling from the fibroblasts was in the immunosuppressive MDSC population. These cells are recruited early during pancreatic tumorigenesis, as they are present at the ADM/PanIN stage and progressively increase during malignant progression [22,60]. Additionally, MDSC levels positively correlate with FoxP3-positive Treg numbers in pancreatic cancer, consistent with our results at the ADM stage [61]. Further functional studies into MDSCs in pancreatic cancer has revealed that pancreatic cancer–associated stellate cells secrete factors that drive MDSC differentiation, which in turn suppresses CD8-positive T-cell proliferation [62]. It has also been observed that MDSC and CD8-positive populations are present in a nearly mutually exclusive relationship in both PanIN and PDAC, suggesting that early host immunosuppressive responses are able to impede T-cell infiltration [22]. The decrease in MDSCs in *Ets2*-deleted pancreata may open the door for recruitment of CD8-positive T cells. These cells have previously been characterized for their ability to eliminate tumor cells during pancreatic cancer development and progression [63], and patients who have increased CD8-positive populations have improved prognosis [64,65]. The genetic data presented here suggest that ETS2 is involved in the interactions between fibroblasts and immunosuppressive cells that may contribute to $Kras^{G12D}$ epithelial cell proliferation indirectly.

$Kras^{G12D}$ epithelial cell proliferation may also be directly affected by ETS2 in fibroblasts, as chemokines are a major conduit of

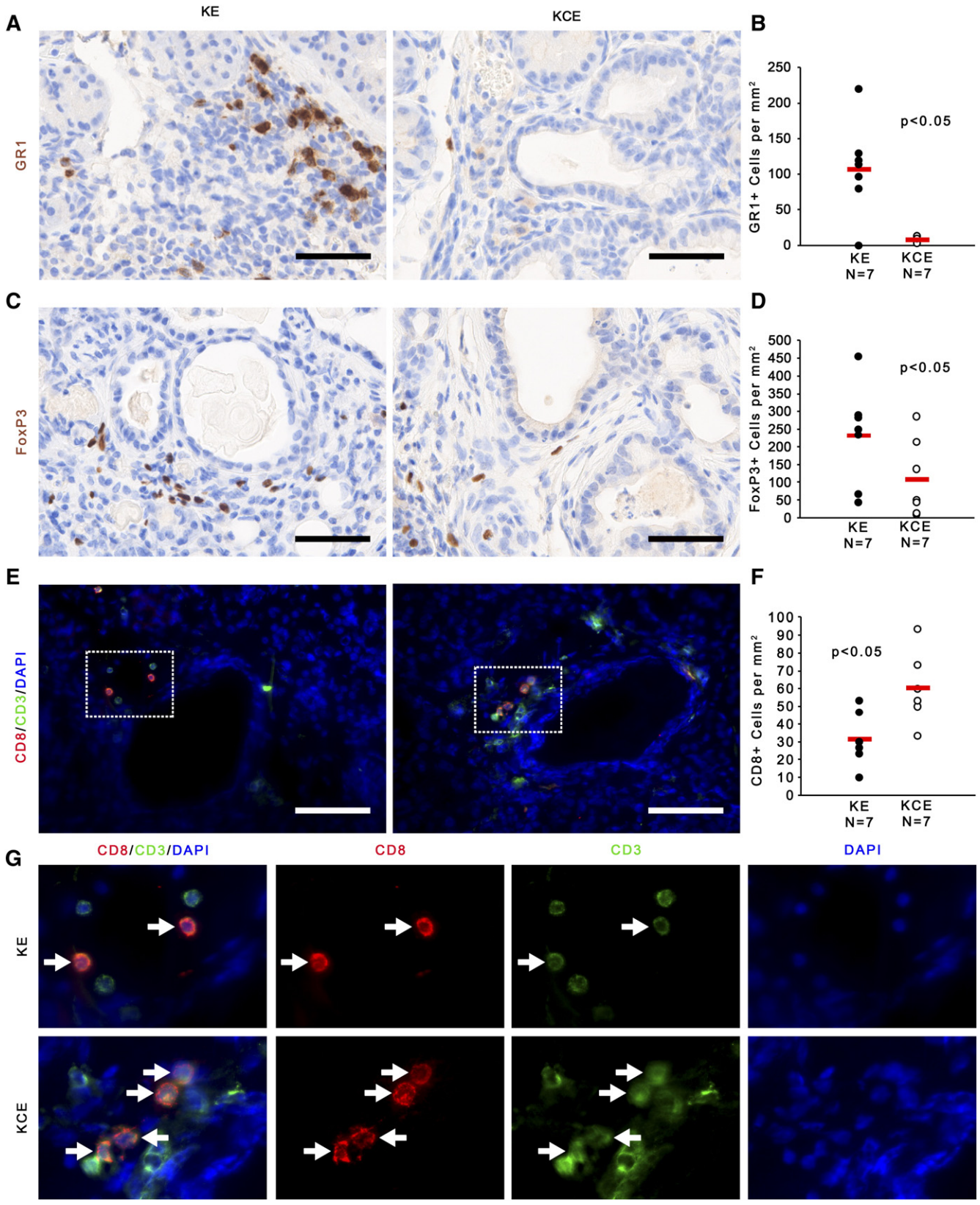

Figure 5. *Ets-2* fibroblast deletion alters the pancreatic immune microenvironment.(A and B) IHC for GR1 (brown) and quantification of positive cells per mm^2. (C and D) IHC for FoxP3 (brown) and quantification of positive cells per mm^2. (E and F) Co-IF for CD8 (red) and CD3 (green) and quantification of CD8-positive cells per mm^2. (G) Insets show higher magnified view of representative areas; white arrows indicate CD3+/CD8+ cells. All scale bars 25 μm (n = 7; red bar indicates mean).

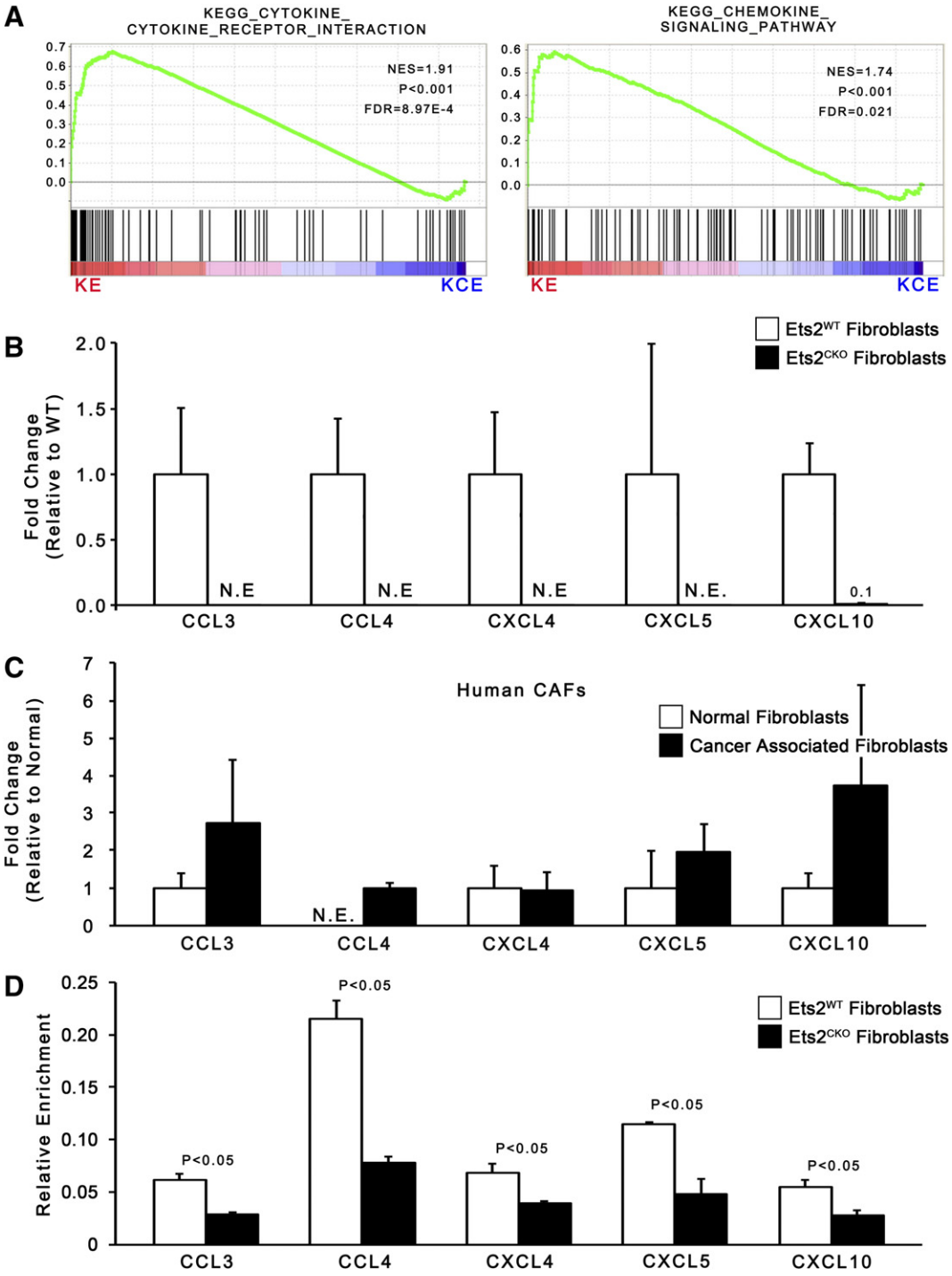

Figure 6. *Ets-2* directly regulates chemokine and cytokine production.(A) GSEA enrichment plots for cytokine and chemokine pathways in KE versus KCE fibroblasts ($n = 3$). (B) qRT-PCR of secreted factors in KE and KCE mouse fibroblasts (normalized to *Rpl4,* represented as fold-change relative to $ETS2^{WT}$ expression; $n = 3$; bars represent means ± SD; N.E. = not expressed). (C) qRT-PCR of secreted factors in human PDAC-derived CAF cultures (normalized to *Rpl4,* represented as fold-change relative to normal fibroblast expression; $n = 3$; bars represent means ± SD). (D) Relative enrichment for ETS2 binding to the promoters of indicated genes in KE and KCE mouse fibroblasts ($n = 5$; bars represent means ± SD).

epithelial-fibroblast communication in the pancreas [63]. The ETS2 targets CCL3, CCL4, CXCL5, and CXCL10 have all been linked to increased tumor cell proliferation in a variety of cancers [66–70]. ETS2 signaling may also play an important signal transduction role from within the epithelial cell, given its role downstream of RAS-MAPK and mutant P53 signaling pathways [38,39,71–73]. Thus, ETS2 could present an overlap between KRAS and p53 signaling, but further biochemical work will be required to pin down the interworkings of this signaling network within the pancreatic tumor cell. Targeting ETS2 signaling may be beneficial to inhibit both epithelial cell intrinsic oncogenic mechanisms as well as the fibroblast-driven immune-modulatory effects defined herein.

Supplementary data to this article can be found online at http://dx.doi.org/10.1016/j.neo.2016.07.006.

Conflict of Interest

The authors report no conflicts of interest.

Acknowledgements

We acknowledge Jason Bice, Daphne Bryant, Nicole Drummond, and Lisa Rawahneh from the OSU Solid Tumor Biology Histology Core for their technical support. We also thank Chelsea K. Martin for assisting in initial analysis of pancreatic tumor histology. We acknowledge the OSUCCC Genomics, Microscopy, Transgenic/Knockout, Target Validation, Analytic Cytometry, Bioinformatics, and Biostatistics Shared Resources. This study was supported by National Institutes of Health grants PO1 CA097189 (M. C. O. and G. L.), NRSA F31 CA189757 (J. R. P.), and R01 CA124586 (S. F. K.). This work was also supported by the Pelotonia Fellowship Program (J. R. P.). Any opinions, findings, and conclusions expressed in this material are those of the author(s) and do not necessarily reflect those of the Pelotonia Fellowship Program.

References

[1] Hidalgo M (2010). Pancreatic cancer. *N Engl J Med* **362**(17), 1605–1617.
[2] Howlader N, Noone AM, Krapcho M, Garshell J, Miller D, Altekruse SF, Kosary CL, Yu M, Ruhl J, and Tatalovich Z, et al (2015). SEER Cancer Statistics Review, 1975-2012. Bethesda, MD: National Cancer Institute; 2015 [http://seer.cancer.gov/csr/1975_2012/, based on November 2014 SEER data submission, posted to the SEER web site].
[3] Almoguera C, Shibata D, Forrester K, Martin J, Arnheim N, and Perucho M (1988). Most human carcinomas of the exocrine pancreas contain mutant c-K-ras genes. *Cell* **53**(4), 549–554.
[4] Barton CM, Staddon SL, Hughes CM, Hall PA, O'Sullivan C, Kloppel G, Theis B, Russell RC, Neoptolemos J, and Williamson RC, et al (1991). Abnormalities of the p53 tumour suppressor gene in human pancreatic cancer. *Br J Cancer* **64**(6), 1076–1082.
[5] Scarpa A, Capelli P, Mukai K, Zamboni G, Oda T, Iacono C, and Hirohashi S (1993). Pancreatic adenocarcinomas frequently show p53 gene mutations. *Am J Pathol* **142**(5), 1534–1543.
[6] Kanda M, Matthaei H, Wu J, Hong SM, Yu J, Borges M, Hruban RH, Maitra A, Kinzler K, and Vogelstein B, et al (2012). Presence of somatic mutations in most early-stage pancreatic intraepithelial neoplasia. *Gastroenterology* **142**(4), 730–733 [e9].
[7] Hezel AF, Kimmelman AC, Stanger BZ, Bardeesy N, and Depinho RA (2006). Genetics and biology of pancreatic ductal adenocarcinoma. *Genes Dev* **20**(10), 1218–1249.
[8] Grippo PJ, Nowlin PS, Demeure MJ, Longnecker DS, and Sandgren EP (2003). Preinvasive pancreatic neoplasia of ductal phenotype induced by acinar cell targeting of mutant Kras in transgenic mice. *Cancer Res* **63**(9), 2016–2019.
[9] Habbe N, Shi G, Meguid RA, Fendrich V, Esni F, Chen H, Feldmann G, Stoffers DA, Konieczny SF, and Leach SD, et al (2008). Spontaneous induction of murine pancreatic intraepithelial neoplasia (mPanIN) by acinar cell targeting of oncogenic Kras in adult mice. *Proc Natl Acad Sci U S A* **105**(48), 18913–18918.
[10] Tuveson DA, Zhu L, Gopinathan A, Willis NA, Kachatrian L, Grochow R, Pin CL, Mitin NY, Taparowski EJ, and Gimotty PA, et al (2006). Mist1-KrasG12D knock-in mice develop mixed differentiation metastatic exocrine pancreatic carcinoma and hepatocellular carcinoma. *Cancer Res* **66**(1), 242–247.
[11] De La OJ, Emerson LL, Goodman JL, Froebe SC, Illum BE, Curtis AB, and Murtaugh LC (2008). Notch and Kras reprogram pancreatic acinar cells to ductal intraepithelial neoplasia. *Proc Natl Acad Sci U S A* **105**(48), 18907–18912.
[12] Kopp JL, von Figura G, Mayes E, Liu FF, Dubois CL, Morris JP, Pan FC, Akiyama H, Wright CV, and Jensen K, et al (2012). Identification of Sox9-dependent acinar-to-ductal reprogramming as the principal mechanism for initiation of pancreatic ductal adenocarcinoma. *Cancer Cell* **22**(6), 737–750.
[13] Eser S, Reiff N, Messer M, Seidler B, Gottschalk K, Dobler M, Hieber M, Arbeiter A, Klein S, and Kong B, et al (2013). Selective requirement of PI3K/PDK1 signaling for Kras oncogene-driven pancreatic cell plasticity and cancer. *Cancer Cell* **23**(3), 406–420.
[14] Zhang Y, Morris JP, Yan W, Schofield HK, Gurney A, Simeone DM, Millar SE, Hoey T, Hebrok M, and Pasca di Magliano M (2013). Canonical wnt signaling is required for pancreatic carcinogenesis. *Cancer Res* **73**(15), 4909–4922.
[15] Liou GY, Doppler H, Necela B, Krishna M, Crawford HC, Raimondo M, and Storz P (2013). Macrophage-secreted cytokines drive pancreatic acinar-to-ductal metaplasia through NF-kappaB and MMPs. *J Cell Biol* **202**(3), 563–577.
[16] Shi G, DiRenzo D, Qu C, Barney D, Miley D, and Konieczny SF (2013). Maintenance of acinar cell organization is critical to preventing Kras-induced acinar-ductal metaplasia. *Oncogene* **32**(15), 1950–1958.
[17] Zhang W, Nandakumar N, Shi Y, Manzano M, Smith A, Graham G, Gupta S, Vietsch EE, Laughlin SZ, and Wadhwa M, et al (2014). Downstream of mutant KRAS, the transcription regulator YAP is essential for neoplastic progression to pancreatic ductal adenocarcinoma. *Sci Signal* **7**(324), ra42.
[18] Maitra A, Fukushima N, Takaori K, and Hruban RH (2005). Precursors to invasive pancreatic cancer. *Adv Anat Pathol* **12**(2), 81–91.
[19] Zhu L, Shi G, Schmidt CM, Hruban RH, and Konieczny SF (2007). Acinar cells contribute to the molecular heterogeneity of pancreatic intraepithelial neoplasia. *Am J Pathol* **171**(1), 263–273.
[20] Parsa I, Longnecker DS, Scarpelli DG, Pour P, Reddy JK, and Lefkowitz M (1985). Ductal metaplasia of human exocrine pancreas and its association with carcinoma. *Cancer Res* **45**(3), 1285–1290.
[21] Remmers N, Anderson JM, Linde EM, DiMaio DJ, Lazenby AJ, Wandall HH, Mandel U, Clausen H, Yu F, and Hollingsworth MA (2013). Aberrant expression of mucin core proteins and o-linked glycans associated with progression of pancreatic cancer. *Clin Cancer Res* **19**(8), 1981–1993.
[22] Clark CE, Hingorani SR, Mick R, Combs C, Tuveson DA, and Vonderheide RH (2007). Dynamics of the immune reaction to pancreatic cancer from inception to invasion. *Cancer Res* **67**(19), 9518–9527.
[23] Collins MA, Bednar F, Zhang Y, Brisset JC, Galban S, Galban CJ, Rakshit S, Flannagan KS, Adsay NV, and Pasca di Magliano M, et al (2012). Oncogenic Kras is required for both the initiation and maintenance of pancreatic cancer in mice. *J Clin Invest* **122**(2), 639–653.
[24] Korc M (2007). Pancreatic cancer–associated stroma production. *Am J Surg* **194**(4 Suppl.), S84–S86.
[25] Feig C, Gopinathan A, Neesse A, Chan DS, Cook N, and Tuveson DA (2012). The pancreas cancer microenvironment. *Clin Cancer Res* **18**(16), 4266–4276.
[26] Neesse A, Algul H, Tuveson DA, and Gress TM (2015). Stromal biology and therapy in pancreatic cancer: a changing paradigm. *Gut* **64**(9), 1476–1484.
[27] Erkan M, Hausmann S, Michalski CW, Fingerle AA, Dobritz M, Kleeff J, and Friess H (2012). The role of stroma in pancreatic cancer: diagnostic and therapeutic implications. *Nat Rev Gastroenterol Hepatol* **9**(8), 454–467.
[28] Perez-Mancera PA, Guerra C, Barbacid M, and Tuveson DA (2012). What we have learned about pancreatic cancer from mouse models. *Gastroenterology* **142**(5), 1079–1092.
[29] Feig C, Jones JO, Kraman M, Wells RJ, Deonarine A, Chan DS, Connell CM, Roberts EW, Zhao Q, and Caballero OL, et al (2013). Targeting CXCL12 from FAP-expressing carcinoma-associated fibroblasts synergizes with anti–PD-L1 immunotherapy in pancreatic cancer. *Proc Natl Acad Sci U S A* **110**(50), 20212–20217.
[30] Rhim AD, Oberstein PE, Thomas DH, Mirek ET, Palermo CF, Sastra SA, Dekleva EN, Saunders T, Becerra CP, and Tattersall IW, et al (2014). Stromal elements act to restrain, rather than support, pancreatic ductal adenocarcinoma. *Cancer Cell* **25**(6), 735–747.
[31] Ozdemir BC, Pentcheva-Hoang T, Carstens JL, Zheng X, Wu CC, Simpson TR, Laklai H, Sugimoto H, Kahlert C, and Novitskiy SV, et al (2014). Depletion of carcinoma-associated fibroblasts and fibrosis induces immunosuppression and accelerates pancreas cancer with reduced survival. *Cancer Cell* **25**(6), 719–734.
[32] Fujita H, Ohuchida K, Mizumoto K, Nakata K, Yu J, Kayashima T, Cui L, Manabe T, OhtsukaTanaka M (2010). alpha-Smooth muscle actin expressing stroma promotes an aggressive tumor biology in pancreatic ductal adenocarcinoma. *Pancreas* .
[33] Moffitt RA, Marayati R, Flate EL, Volmar KE, Loeza SG, Hoadley KA, Rashid NU, Williams LA, Eaton SC, Chung AH, and Smyla JK, et al (2015). Virtual microdissection identifies distinct tumor- and stroma-specific subtypes of pancreatic ductal adenocarcinoma. **47**(10), 1168–1178.
[34] Hollingsworth MA, Yeh JJ, Yang BS, Hauser CA, Henkel G, Colman MS, Van Beveren C, Stavey KJ, Hume DA, Maki RA, and Ostrowski MC (1996). Ras-mediated phosphorylation of a conserved threonine residue enhances the transactivation activities of c-Ets1 and c-Ets2. *Nat Genet* **16**(2), 538–547.
[35] Patton SE, Martin ML, Nelsen LL, Fang X, Mills GB, Bast Jr RC, and OStrowski Jr MC (1998). Activation of the ras-mitogen–activated protein kinase pathway and phosphorylation of ets-2 at position threonine 72 in human ovarian cancer cell lines. *Cancer Res* **58**(10), 2253–2259.

[36] Foulds CE, Nelson ML, Blaszczak AG, and Graves BJ (2004). Ras/mitogen-activated protein kinase signaling activates Ets-1 and Ets-2 by CBP/p300 recruitment. *Mol Cell Biol* **24**(24), 10954–10964.

[37] Kabbout M, Dakhlallah D, Sharma S, Bronisz A, Srinivasan R, Piper M, Marsh CB, and Ostrowski MC (2014). MicroRNA 17-92 cluster mediates ETS1 and ETS2-dependent RAS-oncogenic transformation. *PLoS One* **9**(6)e100693.

[38] Do PM, Varanasi L, Fan S, Li C, Kubacka I, Newman V, Chauhan K, Daniels SR, Boccetta M, and Garrett MR, et al (2012). Mutant p53 cooperates with ETS2 to promote etoposide resistance. *Genes Dev* **26**(8), 830–845.

[39] Xiong S, Tu H, Kollareddy M, Pant V, Li Q, Zhang Y, Jackson JG, Suh YA, Elizondo-Fraire AC, and Yang P, et al (2014). Pla2g16 phospholipase mediates gain-of-function activities of mutant p53. *Proc Natl Acad Sci U S A* **111**(30), 11145–11150.

[40] Kollareddy M, Dimitrova E, Vallabhaneni KC, Chan A, Le T, Chauhan KM, Carrero ZI, Ramakrishnan G, Watabe K, and Haupt Y, et al (2015). Regulation of nucleotide metabolism by mutant p53 contributes to its gain-of-function activities. *Nat Commun* **6**, 7389.

[41] Trimboli AJ, Cantemir-Stone CZ, Li F, Wallace JA, Merchant A, Creasap N, Thompson JC, Caserta E, Wang H, and Chong JL, et al (2009). Pten in stromal fibroblasts suppresses mammary epithelial tumours. *Nature* **461**(7267), 1084–1091.

[42] Wallace JA, Li F, Balakrishnan S, Cantemir-Stone CZ, Pecot T, Martin C, Kladney RD, Sharma SM, Trimboli AJ, and Fernandez SA, et al (2013). Ets2 in tumor fibroblasts promotes angiogenesis in breast cancer. *PLoS One* **8**(8)e71533.

[43] Bronisz A, Godlewski J, Wallace JA, Merchant AS, Nowicki MO, Mathsyaraja H, Srinivasan R, Trimboli AJ, Martin CK, and Li F, et al (2012). Reprogramming of the tumour microenvironment by stromal PTEN-regulated miR-320. *Nat Cell Biol* **14**(2), 159–167.

[44] Man AK, Young LJ, Tynan JA, Lesperance J, Egeblad M, Werb Z, Hauser CA, Muller WJ, CArdiff RD, and Oshima RG (2003). Ets2-dependent stromal regulation of mouse mammary tumors. *Mol Cell Biol* **23**(23), 8614–8625.

[45] Behrens P, Mathiak M, Mangold E, Kirdorf S, Wellmann A, Fogt F, Rothe M, Florin A, and Wernert N, et al (2003). Stromal expression of invasion-promoting, matrix-degrading proteases MMP-1 and -9 and the Ets 1 transcription factor in HNPCC carcinomas and sporadic colorectal cancers. *Int J Cancer* **107**(2), 183–188.

[46] Behrens P, Rothe M, Wellmann A, Krischler J, and Wernert N (2001). The Ets-1 transcription factor is up-regulated together with MMP 1 and MMP 9 in the stroma of pre-invasive breast cancer. *J Pathol* **194**(1), 43–50.

[47] Trimboli AJ, Fukino K, de Bruin A, Wei G, Shen L, Tanner SM, Cresap N, Rosol TJ, Robinson ML, and Eng C, et al (2008). Direct evidence for epithelial-mesenchymal transitions in breast cancer. *Cancer Res* **68**(3), 937–945.

[48] Wei G, Srinivasan R, Cantemir-Stone CZ, Sharma SM, Santhanam R, Weinstein M, Muthusamy N, Man AK, Oshima RG, and Leone G, et al (2009). Ets1 and Ets2 are required for endothelial cell survival during embryonic angiogenesis. *Blood* **114**(5), 1123–1130.

[49] Yamamoto H, Flannery ML, Kupriyanov S, Pearce J, McKercher SR, Henkel GW, Maki RA, Werb Z, and Oshima RG, et al (1998). Defective trophoblast function in mice with a targeted mutation of Ets2. *Genes Dev* **12**(9), 1315–1326.

[50] Yu L, Gulati P, Fernandez S, Pennell M, Kirschner L, and Jarjoura D (2011). Fully moderated T-statistic for small sample size gene expression arrays. *Stat Appl Genet Mol Biol* **10**(1).

[51] Ito Y, Miyoshi E, Takeda T, Sakon M, Ihara S, Tsujimoto M, and Matsuura N, et al (2002). Ets-2 overexpression contributes to progression of pancreatic adenocarcinoma. *Oncol Rep* **9**(4), 853–857.

[52] Walter K, Omura N, Hong SM, Griffith M, Vincent A, Borges M, and Goggins M, et al (2010). Overexpression of smoothened activates the sonic hedgehog signaling pathway in pancreatic cancer-associated fibroblasts. *Clin Cancer Res* **16**(6), 1781–1789.

[53] Yauch RL, Gould SE, Scales SJ, Tang T, Tian H, Ahn CP, Marshall D, Fu L, Januario T, and Kallop D, et al (2008). A paracrine requirement for hedgehog signalling in cancer. *Nature* **455**(7211), 406–410.

[54] Ajuebor MN, Hogaboam CM, Le T, Proudfoot AE, and Swain MG (2004). CCL3/MIP-1alpha is pro-inflammatory in murine T cell–mediated hepatitis by recruiting CCR1-expressing CD4(+) T cells to the liver. *Eur J Immunol* **34**(10), 2907–2918.

[55] Burger JA, Quiroga MP, Hartmann E, Burkle A, Wierda WG, Keating MJ, and Rosenwald A, et al (2009). High-level expression of the T-cell chemokines CCL3 and CCL4 by chronic lymphocytic leukemia B cells in nurselike cell cocultures and after BCR stimulation. *Blood* **113**(13), 3050–3058.

[56] Balamayooran G, Batra S, Cai S, Mei J, Worthen GS, Penn AL, and Jeyaseelan S (2012). Role of CXCL5 in leukocyte recruitment to the lungs during secondhand smoke exposure. *Am J Respir Cell Mol Biol* **47**(1), 104–111.

[57] Petrovic-Djergovic D, Popovic M, Chittiprol S, Cortado H, Ransom RF, and Partida-Sanchez S (2015). CXCL10 induces the recruitment of monocyte-derived macrophages into kidney, which aggravate puromycin aminonucleoside nephrosis. *Clin Exp Immunol* **180**(2), 305–315.

[58] Srivastava K, Cockburn IA, Swaim A, Thompson LE, Tripathi A, Fletcher CA, Shirk EM, Sun H, Kowalska MA, and Fox-Talbot K, et al (2008). Platelet factor 4 mediates inflammation in experimental cerebral malaria. *Cell Host Microbe* **4**(2), 179–187.

[59] Chang HY, Chi JT, Dudoit S, Bondre C, van de Rijn M, Botstein D, and Brown PO (2002). Diversity, topographic differentiation, and positional memory in human fibroblasts. *Proc Natl Acad Sci U S A* **99**(20), 12877–12882.

[60] Pylayeva-Gupta Y, Lee KE, Hajdu CH, Miller G, and Bar-Sagi D (2012). Oncogenic Kras-induced GM-CSF production promotes the development of pancreatic neoplasia. *Cancer Cell* **21**(6), 836–847.

[61] Gabitass RF, Annels NE, Stocken DD, Pandha HA, and Middleton GW (2011). Elevated myeloid-derived suppressor cells in pancreatic, esophageal and gastric cancer are an independent prognostic factor and are associated with significant elevation of the Th2 cytokine interleukin-13. *Cancer Immunol Immunother* **60**(10), 1419–1430.

[62] Mace TA, Ameen Z, Collins A, Wojcik S, Mair M, Young GS, Fuchs JR, Eubank TD, Frankel WL, and Bekaii-Saab T, et al (2013). Pancreatic cancer-associated stellate cells promote differentiation of myeloid-derived suppressor cells in a STAT3-dependent manner. *Cancer Res* **73**(10), 3007–3018.

[63] Wormann SM, Diakopoulos KN, Lesina M, and Algul H (2014). The immune network in pancreatic cancer development and progression. *Oncogene* **33**(23), 2956–2967.

[64] Ademmer K, Ebert M, Muller-Ostermeyer F, Friess H, Buchler MW, Schubert W, and Malfertheiner P, et al (1998). Effector T lymphocyte subsets in human pancreatic cancer: detection of CD8 + CD18+ cells and CD8 + CD103+ cells by multi-epitope imaging. *Clin Exp Immunol* **112**(1), 21–26.

[65] Fukunaga A, Miyamoto M, Cho Y, Murakami S, Kawarada Y, Oshikiri T, Kato K, Kurokawa T, Suzuoki M, and Nakakubo Y, et al (2004). CD8+ tumor-infiltrating lymphocytes together with CD4+ tumor-infiltrating lymphocytes and dendritic cells improve the prognosis of patients with pancreatic adenocarcinoma. *Pancreas* **28**(1), e26–e31.

[66] Tsai SC, Lin SJ, Lin CJ, Chou YC, Lin JH, Yeh TH, Chen MR, Huang LM, Lu MY, and Huang YC, et al (2013). Autocrine CCL3 and CCL4 induced by the oncoprotein LMP1 promote Epstein-Barr virus–triggered B cell proliferation. *J Virol* **87**(16), 9041–9052.

[67] Lentzsch S, Gries M, Janz M, Bargou R, Dorken B, and Mapara MY (2003). Macrophage inflammatory protein 1-alpha (MIP-1 alpha) triggers migration and signaling cascades mediating survival and proliferation in multiple myeloma (MM) cells. *Blood* **101**(9), 3568–3573.

[68] Zheng J, Zhu X, and Zhang J (2014). CXCL5 knockdown expression inhibits human bladder cancer T24 cells proliferation and migration. *Biochem Biophys Res Commun* **446**(1), 18–24.

[69] Kawamura M, Toiyama Y, Tanaka K, Saigusa S, Okugawa Y, Hiro J, Uchida K, Mohri Y, Inoue Y, and Kusunoki M, et al (2012). CXCL5, a promoter of cell proliferation, migration and invasion, is a novel serum prognostic marker in patients with colorectal cancer. *Eur J Cancer* **48**(14), 2244–2251.

[70] Maru SV, Holloway KA, Flynn G, Lancashire CL, Loughlin AJ, Male DK, and Romero IA (2008). Chemokine production and chemokine receptor expression by human glioma cells: role of CXCL10 in tumour cell proliferation. *J Neuroimmunol* **199**(1–2), 35–45.

[71] Wasylyk B, Hagman J, and Gutierrez-Hartmann A (1998). Ets transcription factors: nuclear effectors of the Ras-MAP-kinase signaling pathway. *Trends Biochem Sci* **23**(6), 213–216.

[72] Sharrocks AD (2001). The ETS-domain transcription factor family. *Nat Rev Mol Cell Biol* **2**(11), 827–837.

[73] Zhu J, Sammons MA, Donahue G, Dou Z, Vedadi M, Getlik M, Barsyte-Lovejoy D, Alawar R, Katona BW, and Shilatifard A, et al (2015). Gain-of-function p53 mutants co-opt chromatin pathways to drive cancer growth. *Nature* **525**(7568), 206–211.